ELSEVIER

Journal of Biomechanics 40 (2007) 3598–3606

JOURNAL OF BIOMECHANICS

www.elsevier.com/locate/jbiomech
www.JBiomech.com

A numerical study of the flow-induced vibration characteristics of a voice-producing element for laryngectomized patients

S.L. Thomson[a,*], J.W. Tack[b], G.J. Verkerke[b,c]

[a]Department of Mechanical Engineering, Brigham Young University, 435 CTB, Provo, UT, USA
[b]Department of BioMedical Engineering, University Medical Center Groningen, University of Groningen, The Netherlands
[c]Department of Biomechanical Engineering, University of Twente, The Netherlands

Accepted 6 June 2007

Abstract

A computational model for exploring the design of a voice-producing voice prosthesis, or voice-producing element (VPE), is presented. The VPE is intended for use by laryngectomized patients who cannot benefit from current speech rehabilitation techniques. Previous experiments have focused on the design of a double-membrane voice generator as a VPE. For optimization studies, a numerical model has been developed. The numerical model introduced incorporates the finite element (FE) method to solve for the flow-induced vibrations of the VPE system, including airflow coupled with a mass-loaded membrane. The FE model includes distinct but coupled fluid and solid domains. The flow solver is governed by the incompressible, laminar, unsteady Navier–Stokes equations. The solid solver allows for large deformation, large strain, and collision. It is first shown that the model satisfactorily represents previously published experimental results in terms of frequency and flow rate, enabling the model for use as a design tool. The model is then used to study the influence of geometric scaling, membrane thickness, membrane stiffness, and slightly convergent or divergent channel geometry on the model response. It is shown that physiological allowable changes in the latter three device parameters alone will not be sufficient to generate the desired reduction in fundamental frequency. However, their effects are quantified and it is shown that membrane stiffness and included angle should be considered in future designs.

Keywords: Voice-producing element; Voice prosthesis; Flow-induced vibrations; Finite element model; Total laryngectomy

1. Introduction

1.1. Background

In an advanced stage of laryngeal carcinoma, it is sometimes necessary to surgically remove the complete larynx (see Fig. 1). Since the vocal folds are situated inside the larynx, the most disturbing consequence of the laryngectomy procedure is the loss of a natural way to produce voice.

Options for voice rehabilitation after laryngectomy include alaryngeal speech using electrolarynx devices and tracheo-esophageal (TE) speech; the latter is realized by insertion of a shunt valve in a surgically created TE puncture, enabling airflow from the trachea to initiate vibration of soft tissue structures (pharyngo-esophageal segment) in the esophagus (Fig. 1b). The shunt valve is often referred to as a "voice prosthesis" in literature, but this designation is misleading as these valves do not produce voice, but rather provide a path for air to flow from the trachea to the esophagus when the tracheostoma is closed off. A primary disadvantage of TE speech is the unnaturally low fundamental frequency. This is of particular concern for female laryngectomized patients.

A method of improving speech by laryngectomized patients by incorporating a voice-producing device within the shunt valve has been proposed. Designs have been recently developed and tested (De Vries et al., 2000; Van der Torn et al., 2001; Tack et al., 2006). These designs incorporate a vibrating reed- or membrane-type element within the shunt valve lumen, the structural characteristics

*Corresponding author. Tel.: +1 801 422 4980; fax: +1 801 422 0516.
E-mail address: thomson@byu.edu (S.L. Thomson).

0021-9290/$ - see front matter © 2007 Elsevier Ltd. All rights reserved.
doi:10.1016/j.jbiomech.2007.06.007

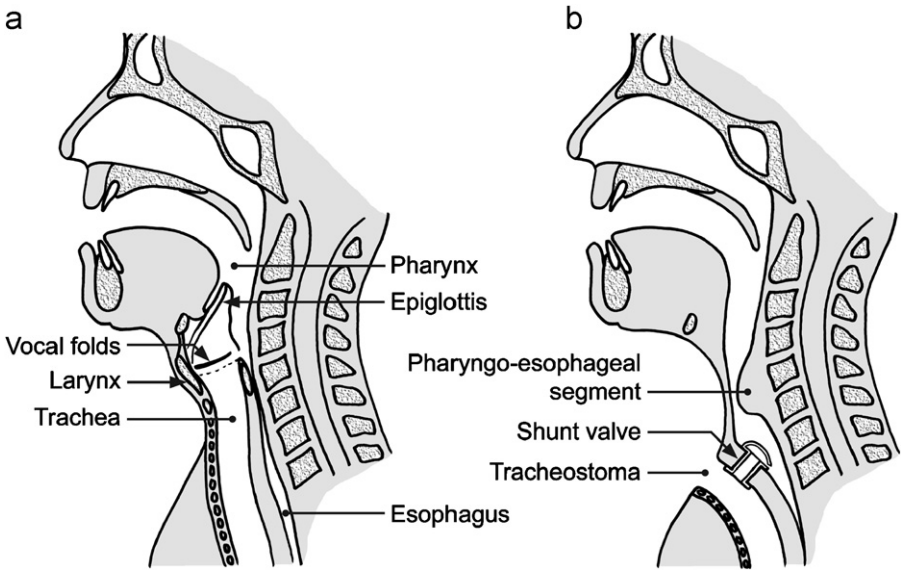

Fig. 1. Illustration showing the situation in the head–neck region (a) of a healthy person, and (b) trachea routing and shunt valve positioning following total laryngectomy.

of which yield flow-induced vibrations at reasonable lung pressures. The most recent design features an approximate fundamental frequency (f_0) of 240 Hz for a lung pressure of about 600 Pa (Tack et al., 2006). This frequency is satisfactory for female speakers. The design also allows for an f_0-lung pressure dependence, which is necessary to prevent a monotonous voice. However, in order for male speakers to benefit from this voice-producing element (VPE), the f_0 of the VPE has to decrease. To find the best way to realize this decrease, a numerical model could be very beneficial.

1.2. Motivation and scope

The current work was a result of efforts to develop a numerical model of the VPE that could be used as a design tool to augment experimental studies. The model was intended to exhibit sufficient agreement with experimental studies so as to be adequate for use as a design tool, while being sufficiently computationally inexpensive to enable the examination of numerous design alternatives. In this paper, we explain the numerical model implementation and report on validation studies. It is shown that the model satisfactorily represents the prototypes in terms of frequency and flow rate. Results of the model sensitivity to a few select design variables are presented and discussed. Implications of model sensitivity to these results are finally discussed.

2. Methods

2.1. Numerical model overview

The VPE prototype, illustrated in Fig. 2, consisted of two membranes stretched within a cylindrical tube. Small weights were attached to the membranes to lower the frequency. When air flowed through the space between the membranes, the membranes self-oscillated.

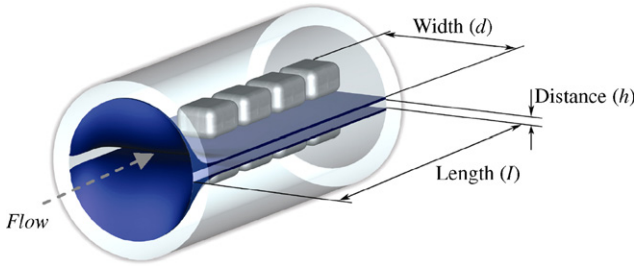

Fig. 2. (Color in online version) Illustration of the experimental VPE prototype.

The new VPE numerical model, shown in Figs. 3–5, consisted of separate but coupled fluid and solid domains to simulate, respectively, the airflow between the membranes and the stretched membrane and attached weights. One-fourth of the VPE was modeled, assuming symmetry about the $z = 0$ and $y = L_{GH}$ planes. The finite element method (Section 2.5) was used for simulations.

2.2. Fluid domain

Numerical values of dimensions and parameters are provided in Table 1. Flow boundary conditions, with u, v, and w as, respectively, the x, y, and z airflow velocity components, were as follows:

(i) Inlet $AA'B'B$: $p = p_s$ (fixed pressure)
(ii) $z = 0$ plane: $w = 0$ m/s (symmetry)
(iii) $y = L_{GH}$ plane: $v = 0$ m/s (symmetry)
(iv) $z = L_{GG'}$ plane: $u = 0$, $v = 0$, $w = 0$ m/s (wall)
(v) Surface $AA'C'C$: $u = 0$, $v = 0$, $w = 0$ m/s (wall)
(vi) Surface $CC'D'D$: $u = 0$, $v = 0$, $w = 0$ m/s (wall)

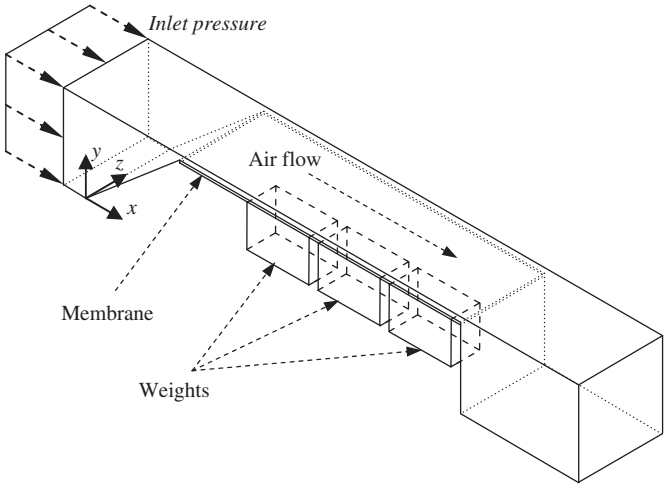

Fig. 3. Schematic of the finite element VPE model.

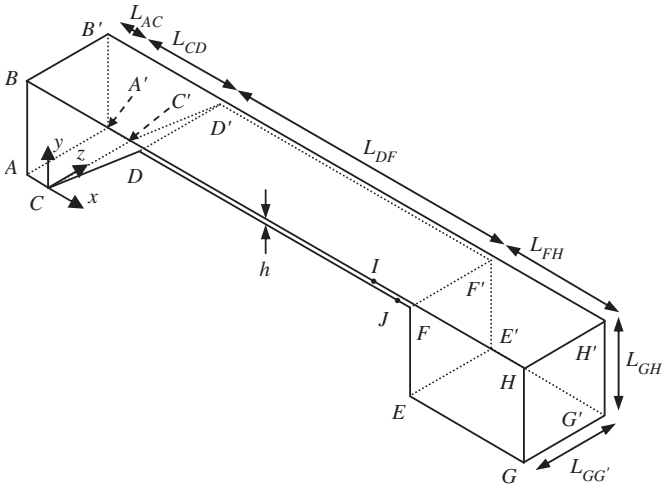

Fig. 4. Finite element model fluid domain.

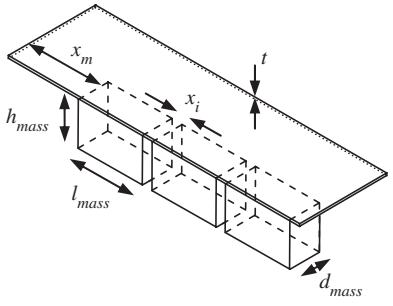

Fig. 5. Finite element model solid domain, including membrane and weights.

(vii)	Surface $DD'F'F$	$u_f = u_s$, $\tau_f = \tau_s$ (equal fluid and solid velocity and traction along wetted membrane surface)
(viii)	Surface $FF'E'E$	$u = 0$, $v = 0$, $w = 0$ m/s (wall)
(ix)	Surface $EE'G'G$	$u = 0$, $v = 0$, $w = 0$ m/s (wall)
(x)	Outlet $GG'H'H$	$p = 0$ Pa (fixed pressure) and $\partial u/\partial x = 0$, $\partial v/\partial x = 0$, and $\partial w/\partial x = 0$ (uniform flow)

Table 1
Numerical domain parameter values for the 2:1 scale models, based on the geometry of the experimental VPE models

Parameter	Description	Value
L_{AC}	Inlet length, straight section	1.25 mm
L_{CD}	Inlet length, convergent section	5 mm
L_{DF}	Membrane length	15 mm
L_{FH}	Outlet length	5.125 mm
L_{GH}	Inlet and outlet section half-height	4.5 mm
$L_{GG'}$	Membrane half-width	4.5 mm
h	Flow channel half-height	0.25 or 0.50 mm
t	Membrane thickness	0.13 mm
h_{mass}	Mass height	2.2 mm
l_{mass}	Mass length	3.3 mm
d_{mass}	Mass half-width	1.5 mm
x_m	Streamwise position of first mass	3.6 mm
x_i	Spacing between masses	0.5 mm
p_s	Inlet pressure	22–1064 Pa
A_{zz}	Initial strain (z-direction)	1.6%

The flow was governed by the laminar, incompressible, unsteady Navier–Stokes equations. The fluid was air with density 1.2 kg/m^3 and dynamic viscosity 1.8×10^{-5} Pa s. Reynolds numbers based on average inlet velocity and inlet surface height ranged from approximately $Re \approx 3 \times 10^2$ at $p_s = 225$ Pa to $Re \approx 10^3$ at $p_s = 1064$ Pa, supporting the laminar flow assumption. Mach numbers were generally less than 0.1, supporting the incompressible flow assumption.

2.3. Solid domain

The upper surface of the membrane was coincident with fluid domain plane $DD'F'F$. The boundary conditions included zero displacement and rotation along the upstream edge ($x = L_{CD}$) and symmetry about the $z = 0$ plane. Along the lateral membrane surface ($z = L_{GG'}$), prescribed z-displacement provided initial strain and the x- and y-displacements were fixed. The downstream surface was unconstrained (except at $z = L_{GG'}$).

The membrane and weights were modeled as three-dimensional volumes. Material geometries and properties were based on the description of Tack et al. (2006). The latex membrane material properties were density 1085 kg/m^3, Poisson's ratio 0.495, and bulk modulus 6.67×10^7 Pa. Values of Young's modulus from 1.5 to 2.5 MPa were explored. The material properties of the three lead weights were density 8437 kg/m^3, Poisson's ratio 0.44, and modulus 16 GPa. The density was slightly lower than that which is typical of lead to account for slight differences in geometry (e.g., rounded-off edges in the prototypes); this brought the FE and prototype masses in closer agreement. Gravitational acceleration of 9.81 m/s^2 in the $-x$ direction was applied to the solid model.

Damping was applied to the model via a Rayleigh proportional damping model. This model is frequently utilized in structural analyses for computational efficiency. The equations of motion for structural analyses are formulated using mass, damping, and stiffness matrices. In the Rayleigh damping model, the damping matrix is calculated as a linear combination of stiffness-proportional and mass-proportional damping, through the use of the model mass and stiffness matrices and two proportionality constants, α and β. These constants are related to the prescribed damping of individual vibration modes of the system. The amount of damping present in the experimental model was not known; in the present study, Rayleigh constants $\alpha = 1.204 \times 10^{-3}$ and $\beta = 7.582 \times 10^{-7}$ were assigned. Further details regarding Rayleigh damping are provided by Bathe (1996) and Hall (2006), and other implementation examples can be found elsewhere (e.g., Hunter et al., 2004; Thomson et al., 2005).

2.4. Fluid–structure interface

The fluid and solid domains were coupled along the membrane surface. Boundary condition (vii) ensured consistent displacement, velocity, and normal stress of the two domains along the interface; consequently, the no-slip fluid condition was also satisfied along the interface.

The experimental results showed that the membranes collided during oscillation. This was found to be the case in the FE model as well. To prevent fluid mesh collapse and subsequent numerical solver failure, contact planes were defined as illustrated in Fig. 6. One contact plane was coincident with the membrane upper surface, and the other was located a distance h_c below the symmetry plane. Collision at this contact plane prevented further collapse of the channel. The distance h_c was defined such that $h_c/h = 0.12$; thus the channel was able to reach 88% closure during vibration. Contact was simulated using the constrain function contact algorithm (Eterovic and Bathe, 1991; Bathe, 1996; ADINA, 2006). The model assumed frictionless contact, included inertial effects leading to collision, and ensured that all kinematic conditions (displacement, velocity, and acceleration) between the contact planes were satisified.

2.5. Numerical approach

The finite element method was applied using the commercial code ADINA (ADINA R&D, Watertown, MA, USA). The fluid domain was meshed using three-dimensional 8-node, brick-shaped, first-order, flow-condition based interpolation elements (Bathe and Zhang, 2004). The weights and membrane were meshed, respectively, using three-dimensional 4-node tetrahedral and 8-node brick elements. The solver allowed for large deformation in all regions, small strain in the weights, and large strains in the membrane.

The fluid equations were solved in a segregated manner. In short, the segregated approach solves for the variables found in the fluid momentum equations (in this case, the three-dimensional unsteady Navier–Stokes equations) and in the continuity (or conservation of mass) equation. In this approach, a scheme for relating pressure and velocity is necessary; in the present study, the SIMPLEC (Van Doormaal and Raithby, 1984) pressure–velocity coupling scheme was applied. The solid equations were solved using a sparse matrix equation solver. Solution of the coupled fluid–solid system was accomplished in an iterative manner.

Time marching was accomplished via the second-order "composite" scheme (ADINA, 2006). At the first few time steps, the initial displacement along the lateral edge of the membrane and the inlet pressure were gradually applied. Simulations continued until relatively stable oscillations were achieved.

Numerical verification studies were performed to verify that the solutions were reasonably accurate with regard to the following factors: grid density, time step size, convergence criteria, and upstream and downstream fluid domain lengths. The following were typical parameters: fluid domain mesh of 2440 elements and 3303 nodes; solid domain mesh of 8906 elements and 7998 nodes; time step size of 125×10^{-6} s (smaller for reduced scale cases; see Section 2.6.2); upstream and downstream lengths as given in Table 1; and all convergence criteria set to 10^{-3}. Model validation was performed by comparing simulation results with the experimental results of Tack et al. (2006) (Sections 2.6.1 and 3.1).

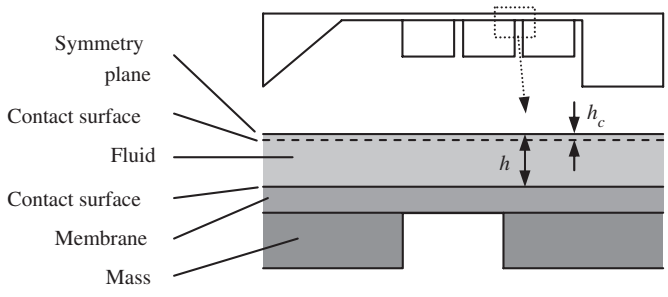

Fig. 6. Cross section of finite element model fluid and solid domains showing contact planes.

2.6. Case studies

Studies were performed for model validation and to investigate the sensitivity of the VPE response to select design variables. The cases were analyzed by comparing vibration frequency, oscillation amplitude, and time-averaged flow rate over a range of inlet pressures.

2.6.1. Validation cases

Tack et al. (2006) investigated several prototypes with different values of inter-membrane fluid channel height ($2h$) and membrane length (L_{DF}) and width ($2L_{GG'}$; factor of 2 because of symmetry). Two cases, referred to in their results as "$h_1l_0d_2$" and "$h_2l_0d_2$", were used for FE model validation. Both cases used the same membrane length ($L_{DF} = 15$ mm) and width ($L_{GG'} = 4.5$ mm), while case $h_1l_0d_2$ used channel height $h = 0.25$ mm and case $h_2l_0d_2$ used $h = 0.5$ mm. The geometries listed in Table 1 correspond to these physical models. Following the experimental tests, five inlet pressures ranging from 225 to 1064 Pa were simulated.

2.6.2. Scaling

Primarily for manufacturing convenience, the experiments of Tack et al. (2006) were achieved using a VPE model that was up-scaled by a factor of two. To predict the model behavior with life-sized dimensions (1:1 scale), the $h_1l_0d_2$ FE studies were repeated with certain geometric and flow parameters reduced to life size, while ensuring dynamic similarity. This was accomplished by linearly decreasing all geometric values by a factor of two, with the exception of the thickness, which was left at $t = 0.13$ mm, and strain was doubled. Details regarding this VPE scaling methodology and rationale can be found in Tack et al. (in review). Material properties were unchanged. The VPE response was investigated at the same values of p_s studied in Section 2.6.1, only increased by a factor of four. Since a four-fold increase in frequency was anticipated (Section 3.2), the time step size for the 1:1 models was reduced to one-fourth to that of the 2:1 models.

2.6.3. Membrane thickness and modulus

Using the FE model, cases with $t = 0.117$ and 0.146 mm ($\pm 10\%$ of nominal) were investigated. All other conditions were the same as for those of case $h_1l_0d_2$. The influence of membrane modulus was also investigated. The prototype membrane modulus was estimated to be 2 MPa. Cases with 1.5 and 2.5 MPa ($\pm 25\%$ of nominal) were investigated. All other conditions were the same as for those in Section 2.6.1.

2.6.4. Included angle

Based largely on a study of the flow-induced vibrations of a membrane in a channel wall (Thomson 2004), it was believed that the included angle of the membrane could significantly influence the model response. Cases were therefore studied with the membrane set at different angles so that the flow region between DD' and FF' formed either a convergent or a divergent channel (see Fig. 7). The initial height of the channel halfway between DD' and FF' was $h = 0.25$ mm, and angles in the range of $\pm 1.5^\circ$ were studied in 0.5° increments (achieved by alternately raising or lowering DD' and FF').

3. Results

3.1. Model validation

In general, the FE model motion compared reasonably well with that observed in the experimental studies of Tack et al. (2006). Fig. 8 shows the membrane system at two times for the $h_1l_0d_2$ case with $p_s = 1064$ Pa. The two images show the membrane during channel closing and maximum

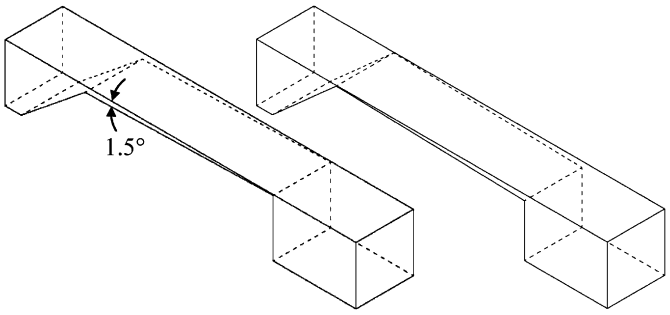

Fig. 7. Geometry for 1.5° convergent (left) and divergent (right) cases.

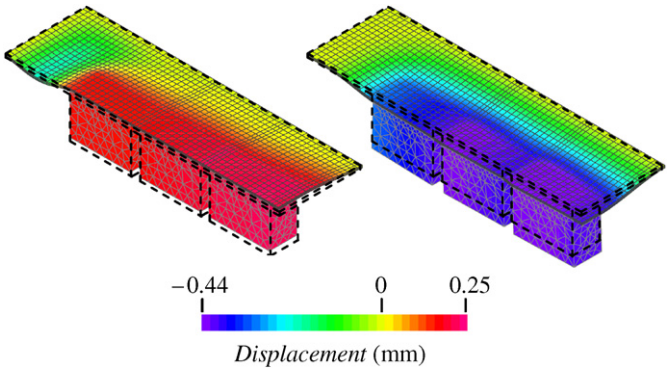

Fig. 8. (Color in online version) Finite element solid domain at two times during oscillation for straight profile case with $p_s = 1064$ Pa and scale 2:1. Color contours denote y-component of displacement. Dashed lines show approximate location of undeformed geometry.

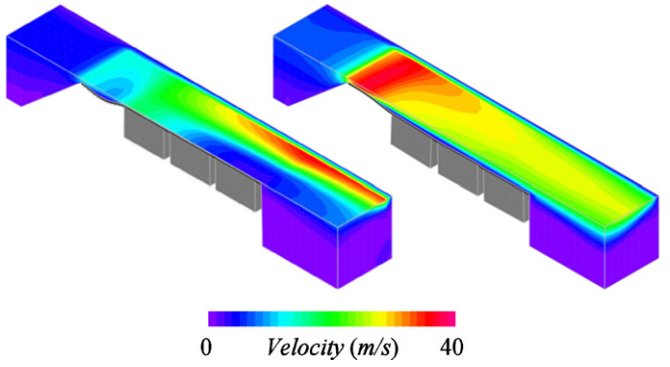

Fig. 9. (Color in online version) x-Component of velocity at two times during oscillation for straight profile case with $p_s = 1064$ Pa and scale 2:1.

opening. Corresponding contours of x-velocity in the fluid domain are shown in Fig. 9. During closing, the velocity in the contact region was very small and the flow was forced primarily through the opening lateral to the weights. During opening the flow was still clearly three dimensional but was more uniform in the spanwise direction.

All driving pressures resulted in self-sustained oscillations; for most pressures, the flow reached a steady-state vibration cycle in 50–150 ms of vibration. This is shown in Fig. 10, where the y-position of the membrane near point J

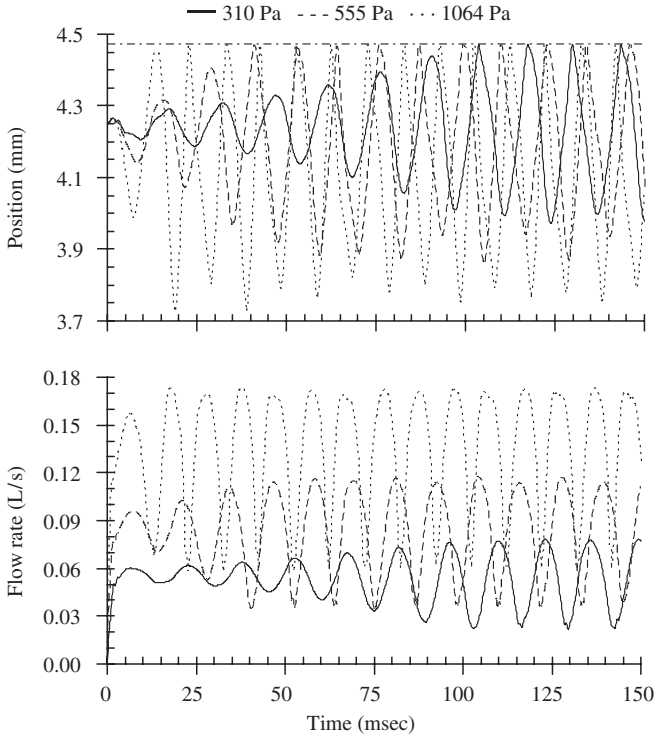

Fig. 10. Membrane y-position and airflow rate vs. time for the $h_1l_0d_2$ case at three different values of p_s; the position is shown for a point approximately identified by point J in Fig. 4. (—) $p_s = 310$ Pa; (- - -) $p_s = 555$ Pa; (· · ·) $p_s = 1064$ Pa; (- · -) contact plane position (top figure only).

(Fig. 4) and the airflow rate are shown for cases of 310, 555, and 1064 Pa.

Fig. 11 shows the dependence of frequency (calculated from a time history of the membrane displacement), average flow rate, and maximum aperture height (amplitude) on pressure for the experimental and computational $h_1l_0d_2$ and $h_2l_0d_2$ cases. The maximum aperture height was defined as twice the maximum y-distance during oscillation between point J and the symmetry plane. The frequency trends are similar and, on average, are within about 13% of the experimental results. It is noted that an *in vacuo* modal analysis performed on the computational $h_1l_0d_2$ case predicted a fundamental frequency of just under 50 Hz; as would be expected, this is lower, but on the same order of magnitude, than the flow-excited frequency of about 70 Hz for the lowest pressure simulated (225 Pa).

The predicted flow rate vs. pressure trends are similar to those measured experimentally, and the computational and experimental data agree to within approximately 8%. A steeper oscillation amplitude vs. pressure slope is seen in the experimental results; discrepancies on the order of 50% of the experimental results are evident. Similar relationships were seen in the $h_2l_0d_2$ cases. The prototype membrane oscillation pattern somewhat resembled that of a streamwise-traveling wave, resulting in a phase difference in displacement between the upstream and

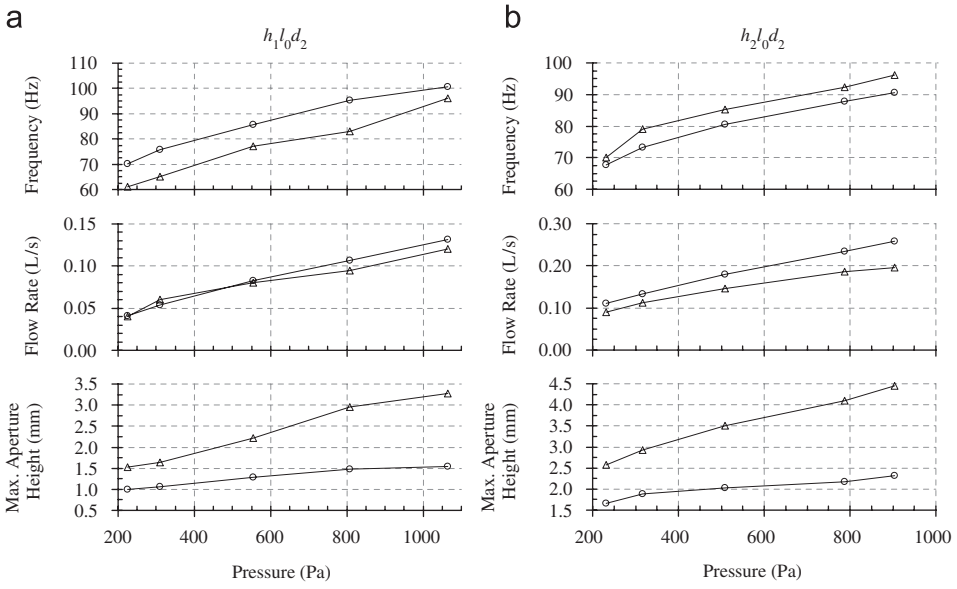

Fig. 11. Frequency, flow rate, and amplitude vs. p_s for the experimental and finite element models: (△) experimental results; (○) FE results.

downstream membrane regions and rather significant mass rotations (particularly at elevated pressures). These features were observed, but were not as pronounced, in the FE model, and the displacement was also lower than that observed in experiments. Reasons for the discrepancies include both numerical and experimental considerations (see Section 4.1). Since the frequency prediction was the primary consideration of the current study, the FE model was deemed satisfactory for evaluating the influence of different design parameters.

3.2. Scaling

Fig. 12 shows frequency, average flow rate, and amplitude vs. pressure for the 2:1 and 1:1 models. The frequency ratio due to scaling ranged from 3.56 to 4.0, with an average of 3.86 across all pressures. The flow rate decreased, on average, by approximately 48%.

3.3. Membrane thickness and modulus

Fig. 13 shows frequency, flow rate, and oscillation amplitude for three membrane thicknesses and five inlet pressures. Frequency increased and amplitude decreased as the thickness increased. Reducing the thickness by 10% resulted in the following: 3.2% decrease in frequency (corresponding to a reduction in frequency of approximately 10 Hz in the 1:1 model), 1.7% increase in flow rate, and 3.7% increase in amplitude.

As shown in Fig. 14, increasing the elasticity modulus resulted in increased frequency and decreased flow rate and amplitude. Reducing the modulus by 25% resulted in the following: 7.1% reduction in frequency (corresponding to a reduction in frequency of approximately 20 Hz in the 1:1 model), 3.9% increase in flow rate, and 5.5% increase in amplitude.

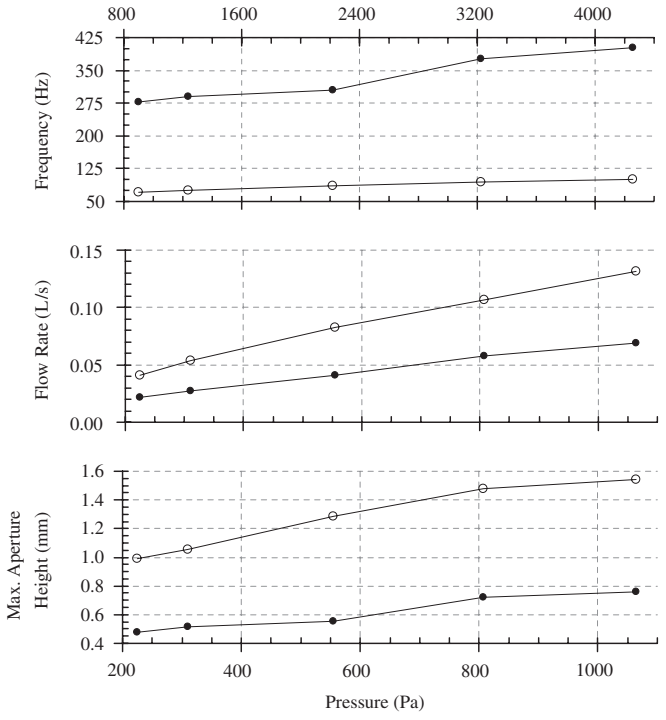

Fig. 12. Frequency, flow rate, and amplitude vs. p_s for 2:1 and 1:1 scale models: (○) 2:1 scale; (●) 1:1 scale.

3.4. Included angle

Results for frequency, flow rate, and amplitude vs. included angle for five pressures are shown in Fig. 15. Not all cases resulted in self-sustained oscillations; for example,

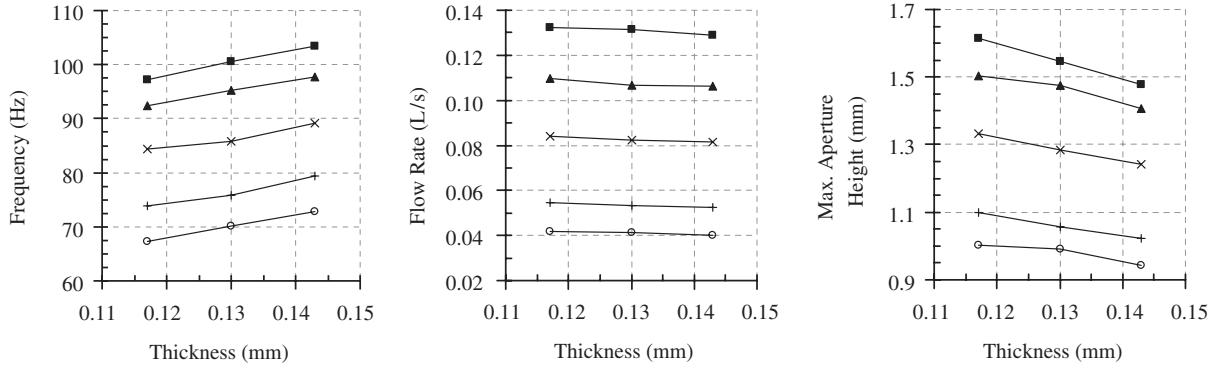

Fig. 13. Frequency, flow rate, and amplitude vs. membrane thickness for different values of p_s for 2:1 scale model: (○) $p_s = 225$ Pa; (+) $p_s = 310$ Pa; (×) $p_s = 555$ Pa; (▲) $p_s = 807$ Pa; (■) $p_s = 1064$ Pa.

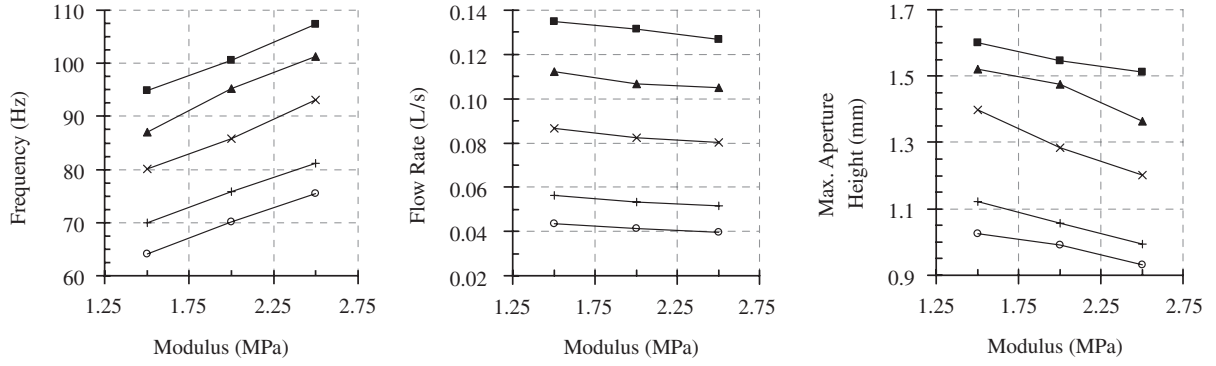

Fig. 14. Frequency, flow rate, and amplitude vs. membrane modulus for different values of p_s for 2:1 scale model. Symbols as per Fig. 13.

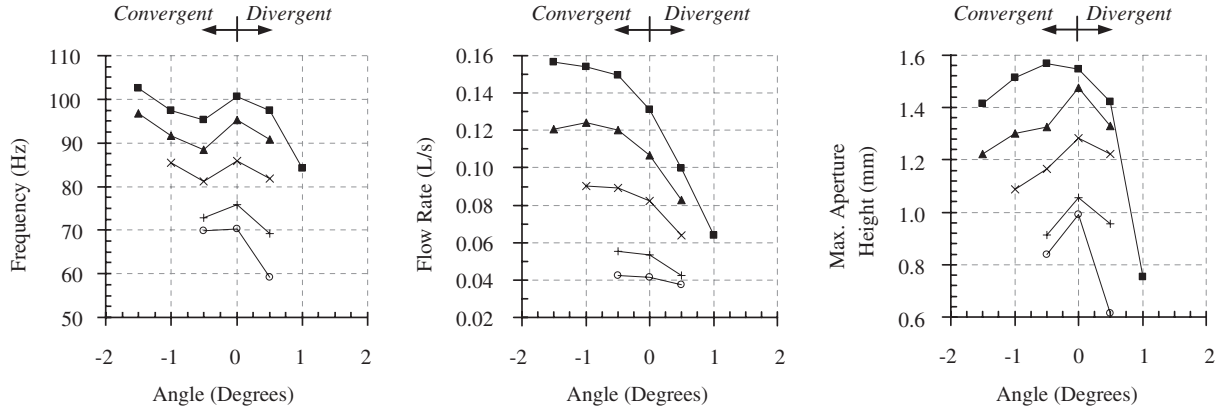

Fig. 15. Frequency, flow rate, and amplitude vs. included angle for different values of p_s for 2:1 scale model. Symbols as per Fig. 13.

for $p_s = 225$ and 310 Pa, only cases with -0.5°, 0°, and $+0.5^\circ$ were self-oscillating. None of the $+1.5^\circ$ cases self-oscillated. The following trends are evident:

(1) Changing to a convergent profile resulted in relatively moderate changes in frequency, oscillation amplitude, and flow rate.
(2) Changing to a divergent profile resulted in reductions in frequency, flow rate, and amplitude; the effect on the latter two quantities was substantial. A change of $+0.5^\circ$ resulted on average in a frequency change of -7.3%.
(3) Changing to a non-zero angle appeared to increase the onset pressure (the onset pressure is the pressure required to initiate vibration). For example, with a $+1^\circ$ geometry, the model vibrations were self-sustained with a 1064 Pa driving pressure, but not with a 807 Pa driving pressure; therefore, the onset pressure would be between 807 and 1064 Pa.

4. Discussion

4.1. Model validation

Given the similarity between the FE results and the experimental results of Tack et al. (2006) in terms of qualitative motion and frequency and flow rate vs. pressure dependence, the model was deemed to be adequate for initial design analysis. Possible reasons for observed discrepancies, particularly in displacement, include numerical and experimental considerations, such as, uncertainty in material properties, variations in prototype fabrication contributing to experimental uncertainty (for example, it was not uncommon for two physical models of the same geometrical configuration to exhibit differences in frequency of around 5–10% and in flow rate around 15–25% for similar driving pressures), simplification in membrane upstream boundary conditions, and unmodeled physical effects (e.g., acoustical loading, vibration-induced material relaxation, and variations in upstream pressure). It is noted that the damping model employed was deemed to be one of the most significant contributors to the observed differences. The present model assumed constant Rayleigh damping coefficients in both membrane and weight regions for all cases. Analyses of unpublished VPE model simulations have demonstrated that the choice of Rayleigh damping coefficient values significantly influenced the model response. For example, reducing the coefficients overall and applying even lower coefficients to the weight regions resulted in greater oscillation amplitude, but also tended to make the model more unstable because of the presence of higher frequency harmonics. It is likely that the prototype possessed lower damping than the present FE model, and further investigation into the influence of damping on the FE model is necessary.

4.2. Scaling

Tack et al. (2006, in review) predicted that relative to a 2:1 model, the frequency of a 1:1 model should increase by a factor of 4 and the flow rate should decrease by a factor of 2. These predictions corresponded well with the FE model's simulated increase in frequency (factor of 3.86) and decrease in flow rate (48%). The 1:1 FE model was predicted to vibrate around 277 Hz for the lowest pressure; this is much too high for males and still high, but almost appropriate, for females.

Additional simulations were performed with a slightly alternate downscaling procedure: the membrane thickness was reduced by 50% and the strain was left the same. This resulted in an average factor of 2.8 increase in frequency (about 183 Hz for the lowest pressure). From a frequency standpoint such a downscaled prototype is favorable, but requires a very thin membrane (65 μm) that may be difficult to fabricate, operate, and maintain.

4.3. Membrane thickness and modulus

A lower vibration frequency could be achieved by decreasing thickness and/or modulus, since both led to a reduction in membrane stiffness. Neither changes in thickness nor modulus alone would be sufficient to enact the necessary reduction in frequency. However, these changes may be helpful when combined with an included angle (discussed below).

4.4. Included angle

A convergent profile resulted in moderate changes in frequency and amplitude, but required larger flow rates. Because the flow rates are low as compared to values measured during normal phonation (0.05–0.351/s; Schutte 1980), a convergent profile would generally be helpful when the low allowable flow rates will prove problematic *in-vivo*. A divergent profile resulted in significant reductions in frequency, flow rate, and amplitude, but at the expense of a higher onset pressure. For example, the $+1.0^{\circ}$ orifice resulted in frequencies of about 84 Hz at $p_s = 1064$ Pa, or about 15% lower than the frequencies for a straight profile. However, the onset pressure was between 807 and 1064 Pa. For a 1:1 model, this corresponds to about 336 Hz with an onset pressure between 2.2 and 3.2 kPa; neither of these parameters are satisfactory (1–1.5 kPa is typical for loud conversational speech; Schutte, 1980; Titze, 2000). Thus while a divergent profile yields beneficial results from a frequency standpoint, the benefit is negated by the corresponding increase in onset pressure. The larger onset pressure likely results from the increased viscous losses that are present within the inter-membrane gap. Increasing the overall inter-membrane gap slightly may reduce the onset pressure by reducing the viscous losses (Lucero, 1996, 1998). Thus, a divergent profile with a larger inter-membrane spacing may be beneficial.

4.5. Future work

Areas of future work include further model refinement and VPE design improvement. As mentioned above, damping is a significant factor and a focused study on its influence on the model response would improve overall understanding of the model behavior and potentially yield improved agreement between the model and experimental results. Further refinement includes modeling the flow as a compressible fluid to model acoustic effects and predict radiated sound (enabling comparison with corresponding experimental data). Other areas of interest include: exploring the influence of asymmetry between the two membranes, further investigation of initial strain, and exploring design alternatives using formal engineering-based optimization methods.

Conflict of interest

None of the authors has a conflict of interest regarding this manuscript.

Acknowledgment

This work was supported in part by NIH Grant NIDCD R01 DC05788.

References

ADINA, 2006. ADINA Theory and Modeling Guide, vol. III: ADINA-F. ADINA R&D Inc.

Bathe, K.J., 1996. Finite Element Procedures. Prentice-Hall, Engleword cliffs, NJ.

Bathe, K.J., Zhang, H., 2004. Finite element developments for general fluid flows with structural interactions. International Journal for Numerical Methods in Engineering 60, 213–232.

De Vries, M.P., van der Plaats, A., van der Torn, M., Mahieu, H.F., Schutte, H.K., Verkerke, G.J., 2000. Design and in vitro testing of a voice-producing element for laryngectomized patients. The International Journal of Artificial Organs 23 (7), 462–472.

Eterovic, A., Bathe, K.J., 1991. On the treatment of inequality constraints arising from contact conditions in finite element analysis. Journal of Computers and Structures 40 (2), 203–209.

Hall, J.F., 2006. Problems encountered from the use (or misuse) of Rayleigh damping. Earthquake Engineering and Structural Dynamics 35, 525–545.

Hunter, E.J., Titze, I.R., Alipour, F., 2004. A three-dimensional model of vocal fold abduction/adduction. Journal of the Acoustical Society of America 115 (4), 1747–1759.

Lucero, J.C., 1996. Relation between the phonation threshold pressure and the prephonatory glottal width in a rectangular glottis. Journal of the Acoustical Society of America 100 (4), 2551–2554.

Lucero, J.C., 1998. Optimal glottal configuration for ease of phonation. Journal of Voice 12 (2), 151–158.

Schutte, H.K., 1980. The efficiency of voice production. Ph.D. Thesis, University of Groningen, Groningen, 194pp.

Tack, J.W., Verkerke, G.J., van der Houwen, E.B., Mahieu, H.F., Schutte, H.K., 2006. Development of a double-membrane sound generator for application in a voice-producing element for laryngectomized patients. Annals of Biomedical Engineering 34, 1896–1907.

Tack, J.W., Hirschberg, A., Schutte, H.K., Mahieu, H.F., van der Houwen, E.B., Verkerke, G.J. Influence of scale on the flow-induced oscillations of a membrane-based sound generator. Journal of Biomechanics, in review.

Thomson, S.L., 2004. Fluid–structure interactions within the human larynx. Ph.D. Dissertation, Purdue University, West Lafayette.

Thomson, S.L., Mongeau, L., Frankel, S.H., 2005. Aerodynamic transfer of energy to the vocal folds. Journal of the Acoustical Society of America 118 (3), 1689–1701.

Titze, I.R., 2000. Principles of Voice Production, second printing. National Center for Voice and Speech, Denver.

van der Torn, M., de Vries, M.P., Festen, J.M., Verdonck-de Leeuw, I.M., Mehieu, H.F., 2001. Alternative voice after laryngectomy using a sound-producing voice prosthesis. Laryngoscope 111 (2), 336–346.

van Doormaal, J.P., Raithby, G.D., 1984. Enhancements of the SIMPLE method for predicting incompressible fluid flows. Numerical Heat Transfer 7 (2), 147–163.